ELSEVIER

Journal of Atmospheric and Solar-Terrestrial Physics 66 (2004) 1057–1073

Journal of ATMOSPHERIC AND SOLAR-TERRESTRIAL PHYSICS

www.elsevier.com/locate/jastp

# A dynamic global model of the plasmasphere

P.A. Webb*, E.A. Essex[1]

*Cooperative Research Centre for Satellite Systems, Department of Physics, La Trobe University, Victoria 3086, Australia*

Received 5 November 2002; received in revised form 3 November 2003; accepted 20 April 2004

**Abstract**

The three-dimensional Global Plasmasphere Ionosphere Density (GPID) model simulates the global-scale dynamics of the magnetic field-aligned ion and electron densities within the plasmasphere and plasmatrough ($L \leqslant 9$) by simultaneously modeling the field-aligned plasma density distributions of several thousand magnetic flux tubes distributed uniformly about the Earth. GPID uses a dynamical diffusive equilibrium approach within each magnetic flux tube that allows it to model the temporal variations in $H^+$ and $O^+$ densities, the dominant ions in the topside ionosphere and plasmasphere. Using the International Reference Ionosphere (IRI) to model the ionosphere and a simple electron density profile above the ionosphere in the polar regions ($L > 9$), GPID is able to simulate electron densities globally from ground level to an altitude of $\sim 50,000$ km. Comparisons of GPID predictions with (1) direct plasmaspheric observations obtained from Low Earth Orbit (LEO) satellites equipped with Global Position System (GPS) receivers, (2) ground-based radio beacon measurements using the Applications Technology Satellite 6 (ATS-6) satellite and (3) several empirical plasmasphere models, show good agreement. This good agreement indicates the value of the GPID model as a tool for investigating the physics of the inner magnetopshere.


*Keywords:* Plasmasphere; Electron density; Modelling; TEC; GPS; ATS-6

## 1. Introduction

With the recent full deployment of the Global Positioning System (GPS) satellite constellation and the continuing reduction in the costs of GPS receivers, ionospheric studies are increasingly conducted with GPS-derived total electron content (TEC) measurements (e.g., Doherty et al., 1997; Mannucci et al., 1999; Horvath and Essex, 2000). These measurements are obtained by observing phase changes in the GPS-transmitted radio signals (e.g., Hofmann-Wellenhof et al., 1997). Because the GPS satellites orbit at 20,200 km, most of the propagation path of a radio signal from a GPS satellite to a ground-based or Low Earth Orbit (LEO) satellite-based GPS receiver is typically within the plasmasphere. But the effect of the plasmasphere on the propagation and, hence, the TEC has been little studied and it is not clear how important the plasmaspheric content is compared to the ionospheric TEC, which is often the parameter that researchers are trying to measure. While many theoretical modeling studies have been conducted on the plasmasphere (e.g., Torr et al., 1990; Wilson et al., 1992; Singh and Horwitz, 1992; Bailey et al., 1997; Tu et al., 2003), investigations of the plasmaspheric TEC contribution have been limited (e.g., Poulter et al., 1981; Lunt et al., 1999a).

Electron densities ($n_e$) in the plasmasphere are several orders of magnitude less than in the underlying ionosphere (e.g., Carpenter and Anderson, 1992). Consequently, the plasmasphere is often ignored when analysing GPS TEC measurements. Nevertheless, due to the large propagation distance through the low-density plasmasphere, compared to the relatively short signal path length through the thin but higher density ionosphere, the plasmaspheric contribution to a ground-based TEC measurement can actually be as high as $\sim$10% during the day and $\sim$40% at night (Davies, 1980). GPS satellite TEC studies have shown that the plasmaspheric

* Corresponding author. Nomad Research, Inc., Laboratory for Extraterrestrial Physics, Code 690, NASA/GSFC, Greenbelt, Maryland 20771, USA.

*E-mail address:* pwebb@lepvax.gsfc.nasa.gov (P.A. Webb).

[1] Deceased 21 March 2004.

1364-6826/$ - see front matter © 2004 Elsevier Ltd. All rights reserved.
doi:10.1016/j.jastp.2004.04.001

TEC is often 3 TEC units (TECU) or more (e.g., Ciraolo and Spalla, 1997; Lunt et al., 1999b), while Applications Technology Satellite 6 (ATS-6) satellite TEC studies from geostationary orbit indicated plasmaspheric TEC as high as 3–8 TECU (e.g., Kersley and Klobuchar, 1980). Furthermore, the nighttime plasmaspheric GPS TEC values of $\sim 1$ TECU can be comparable to the nighttime ionospheric TEC values (e.g., Lunt et al., 1999a). Thus, the plasmaspheric contribution should not be ignored in ionosphere–plasmasphere studies. Since every receiver has its own specific geometry relative to the GPS satellite orbital planes, data from each will include different contributions from the plasmasphere.

Polar region $n_e$'s are similar to those in the plasmatrough (e.g., Nsumei et al., 2003), which are generally one to two orders of magnitude less dense than in the plasmasphere (e.g., Carpenter and Anderson, 1992; Gallagher et al., 2000). As such, the polar and plasmatrough $n_e$ contributions to a GPS TEC observation are small compared to those contributions from the plasmasphere, and almost insignificant compared to those from the ionosphere. Nevertheless, to extract the desired ionospheric information from GPS TEC data sets a global $n_e$ model is required so that the size of TEC contributions of the different regions can be investigated, as well as allowing for the possibility of future comparison between GPID predictions and satellite $n_e$ measurements. This model needs to include both the polar regions ($L > 9$, where $L$ is the McIlwain parameter (McIlwain, 1961)) and the plasmasphere/plasmatrough region ($L < 9$), where the latter will be simply referred to as the plasmasphere in this discussion. From this model the plasmaspheric/polar TEC can be calculated permitting it to be removed from GPS TEC derived measurements, so allowing the ionospheric TEC to be obtained. Furthermore, it allows the dynamics and properties of the plasmasphere to be investigated under varying geomagnetic conditions.

The advantage of a theoretical model, as opposed to an empirical one (e.g., Gallagher et al., 2000), is that it can simulate a wider range of dynamic processes that exist in the plasmasphere; the most important being the emptying by geomagnetic storms followed by refilling from the underlying ionosphere (e.g., Singh and Horwitz, 1992; Carpenter and Lemaire, 1997). The disadvantage with physical models in the past has been their greater demand on computational resources, which has generally restricted their use to mainframe or workstation computers (e.g., Rasmussen et al., 1993). With the rapid increase in the processing power of desktop personal computers in the past decade it is now a practical proposition to model the global plasmasphere on a PC. This possibility was the impetus for the development of the Global Plasmasphere Ionosphere Density (GPID) model.

To produce a global plasmasphere model that can be run on a desktop computer, a variety of assumptions and simplifications were required. The most important ones used in GPID are: (1) International Reference Ionosphere (IRI) (Bilitza, 2001) is used to model the ionosphere, (2) neutral parameters are obtained from the Mass Spectrometer and Incoherent Scatter (MSIS) model (Hedin, 1991; Picone et al., 2002), (3) the Titheridge temperature model (TTM) (Titheridge, 1998; Webb and Essex, 2003) is used to determine the electron and ion temperatures ($T_e$ and $T_i$), (4) an offset centered dipole is used to represent the Earth's magnetic field (Kivelson and Russell, 1995), (5) the plasmaspheric ions are assumed to consist of only $O^+$ and $H^+$, (6) the dynamic diffusive equilibrium approach described in Webb and Essex (2001) is used to model the field-aligned $H^+$ and $O^+$ distribution, (7) the magnetospheric equatorial electric field is given by the McIlwain E5D model (McIlwain, 1986), (8) plasma motion in the equatorial plane is controlled by $\mathbf{E} \times \mathbf{B}$ motion, and (9) the polar regions field aligned electron densities can be modeled using a simple empirical relationship. The use of these assumptions will be described in the following sections.

## 2. Modeling the plasma within a single magnetic flux tube

Webb and Essex (2001) describes the approach used by GPID to simulate the plasma distribution and evolution in a single corotating field-aligned magnetic flux tube. In this approach the total $H^+$ content ($H^+_{tot}$) of the magnetic flux tube is used as the primary conserved parameter. As indicated in Webb and Essex (2001), the model is dynamic even though in one time step ($\Delta t$) the equations are time independent since GPID advances the simulation $\Delta t$ in time and recalculates the changes in the plasmasphere based on the input parameters for the new time.

In each $\Delta t$ of 1 h duration the equatorial $H^+$ number density ($n_{eq}(H^+)$) is estimated via dividing $H^+_{tot}$ by the volume of the magnetic flux tube. A $\Delta t$ of 1 h was chosen because it is short enough to allow GPID to give good agreement with the magnetic flux tube refilling predictions of the more physical complete theoretical field line interhemispheric plasma (FLIP) model (Torr et al., 1990; Richards et al., 2000), but not so small as to result in overly long computation times.

Diffusive equilibrium is then used to determine the $H^+$ number density $n(H^+)$ profile starting from $n_{eq}(H^+)$ down the field line into each hemisphere. Diffusive equilibrium is used for the $O^+$ number density ($n(O^+)$) in both hemispheres, calculated up the magnetic field lines from topside ionosphere whose densities are modeled by the IRI (Bilitza, 2001) up to 50 km above the local F2 $n_e$ peak, as determined by the IRI. Comparisons have shown that a diffusive equilibrium profile, modified at low altitudes to match a chemical equilibrium profile, shows excellent agreement with the FLIP model (Webb and Essex, 2001). The required $T_e$ and $T_i$ are obtained from the TTM (Titheridge, 1998), which has recently been modified (Webb and Essex, 2003). Neutral parameters, such as the H and O densities, are obtained from the MSIS model (Hedin, 1991; Picone et al., 2002). Once

the $n(H^+)$ and $n(O^+)$ profiles are determined, $H^+$ chemical production and loss are calculated along the field line, as well as diffusive $H^+$ loss into the northern and southern topside ionosphere; the flux tube's $H^+_{tot}$ is then modified by the net value of these production and loss processes multiplied by $\Delta t$ to give a new $H^+_{tot}$ at the end of the time step.

The simulation then advances $\Delta t$, moving the plasma in the magnetic flux tube under the assumption of corotation in the magnetic equatorial plane, and then repeats the above steps. Each flux tube's $H^+_{tot}$ will vary with time to reflect changes in the underlying ionosphere, neutral atmosphere, and plasma temperature, which all vary with local time, season, solar conditions, and geomagnetic activity.

This approach results in a magnetic flux tube whose $H^+_{tot}$, and hence $n(H^+)$ distribution, evolves with time to reflect changing geomagnetic and ionospheric conditions. Webb and Essex (2001) showed that this approach can be used to successfully reproduce magnetic flux tube refilling results obtained from the FLIP model, and a close agreement between GPID and whistler-based refilling observations. Furthermore, Webb and Essex (2001) showed the dynamic diffusive equilibrium approach was able to accurately model the diurnal variation in $H^+$ flux observed from whistler observations that at $L = 2.5$, for example, are of the order of 20% of the total $H^+$ content of the magnetic flux tube.

This paper describes the approach GPID uses to produce a global three-dimensional representation of the plasmasphere by modeling the plasma in several thousand magnetic flux tubes distributed about the Earth. The three-dimensional GPID representation no longer assumes corotation, but instead uses $\mathbf{E} \times \mathbf{B}$ drift to determine the motion of the plasma. With the inclusion of a simple $n_e$ magnetic field aligned profile for the polar regions, GPID is able to model $n_e$ globally under a variety of spatial and temporal conditions up to an altitude of $\sim 50,000$ km. Comparisons will be presented between GPID and GPS-derived direct plasmaspheric TEC observations, geostationary ATS-6 Faraday rotation-derived plasmaspheric TEC observations, and several empirical plasmasphere models.

## 3. Global plasmasphere model

### 3.1. E5D electric field model

The global-scale motion of plasmaspheric plasma results from the superposition of corotation with the Earth and the night to day magnetospheric plasma flow from the magnetotail (Nishida, 1966; Brice, 1967); these motions occur due to $\mathbf{E} \times \mathbf{B}$ drift. The bulk three-dimensional motion of the plasmasphere can be obtained by considering the plasma motion in the magnetic equatorial plane, and then projecting this motion along the magnetic field lines into each hemisphere. GPID uses a dipole magnetic field to determine $\mathbf{B}$ and $\mathbf{E}$ is determined from the McIlwain E5D electric field model (McIlwain, 1986), which is modified as described below.

Defining the magnetic longitude to be $\theta = 15^\circ \times$ MLT, where MLT is magnetic local time, the E5D electric field model potential $G$ (measured in kV) in the magnetic equatorial plane is given by

$$G = G_1 G_2 J + G_3, \tag{1}$$

$$G_1 = \{R[V_1 \sin(\theta) + V_2 \cos(\theta)] + V_3\}, \tag{2}$$

$$G_2 = (1 + V_4 K_r), \tag{3}$$

$$G_3 = -V_5/R, \tag{4}$$

$$K_r = \left[\frac{K_p}{1 + 0.1K_p}\right], \tag{5}$$

$$J = \frac{1}{1 + (V_6 R_{ar}/R)^\gamma}, \tag{6}$$

$$R_{ar} = S_1 + S_2 \cos(\theta) + [S_3 + S_4 \cos(\theta)]K_r, \tag{7}$$

$V_1 = 0.8$ $\quad \gamma = 8$

$V_2 = 0.2$ $\quad S_1 = 9.8$

$V_3 = 3.0$ $\quad S_2 = -1.4$

$V_4 = 0.3$ $\quad S_3 = -0.9$

$V_5 = 89.75$ $\quad S_4 = -0.3$

$V_6 = 0.8$

where $R$ is radial distance in Earth radii ($R_E$), $V_i$ are in kV/$R_E$, $S_i$ are in $R_E$, $R_{ar}$ is the location of the auroral ring in $R_E$, and $K_p$ is the geomagnetic index. Note that in the magnetic equatorial plane $R = LR_E$. $V_5$ has been slightly modified from its original value of 92.0 kV/$R_E$, so that the plasma on a dipole magnetic field line at low $L$ completes one orbit in exactly 24 h.

$J$ represents shielding effects that are observed to occur in the region of the auroral oval ($J$ was denoted by $H$ in McIlwain (1986), but changed here because $H$ is used for scale height in the GPID model). Corotation dominates inside $R_{ar}$, while outside the sunward magnetospheric flow is dominant. $J$ controls the position of the transition from the one regime to the other, as a function of $R$ and $K_p$.

While the E5D is an improvement over the simple cross-tail plus corotation $\mathbf{E}$ field model (e.g., Kivelson and Russell, 1995) or the Volland–Stern model (Volland, 1973; Stern, 1975), it still has some weaknesses, e.g., not being accurate during substorms (McIlwain, 1986). Furthermore, because the E5D is based on average geosynchronous satellite data, during changing geomagnetic conditions it does not capture well global scale process such as overshielding recently observed by the EUV Imager on the Imager for Magnetopause-to-Aurora Global Exploration (IMAGE) satellite (Goldstein et al., 2002). The E5D, however, does have the advantage of being computationally simple, and a number of studies have show its accuracy in reproducing the

global **E** field (e.g., Lemaire and Gringauz, 1998; Liemohn et al., 2001). For these reasons, the E5D is used by GPID. A future improvement to GPID would be to include a more physically realistic equatorial **E** field model, such as the Magnetospheric Specification Model (e.g., Goldstein et al., 2003b).

### 3.2. Modifications to the E5D $K_p$ scaling factor

Liemohn et al. (2001) introduced a modification to the scaling factor $G_2$ used by the E5D model. This modification, denoted by $K_L$, is given by

$$K_L = \frac{E_0}{\max[E_M]}, \tag{8}$$

where $E_0$ is the magnetospheric dawn–dusk electric field in kV/$R_E$ (equal to the cross polar cap potential difference divided by the dawn to dusk width of the magnetosphere in the magnetic equatorial plane) and $\max[E_M] = \sqrt{V_1^2 + V_2^2}$. From fits to $E_0$ storm time data based on AMIE potentials (Liemohn et al., 2001) and a magnetopause model (Shue et al., 2000), the following relationship between $E_0$ and the previous 3-hourly $K_p$ in kV/$R_E$ was found (Webb and Liemohn, 2004)

$$E_0(K_p) = 0.0084K_p^3 - 0.0292K_p^2 + 0.3911K_p + 0.5363. \tag{9}$$

Eq. (9) allows Eq. (8) to be estimated using only $K_p$, without requiring information on parameters such as the solar wind pressure. For the GPID results presented here, $K_L$ is used in place of the $G_2$ scaling factor.

Only limited data were available for $K_p > 7$, so Eq. (9) should be used with caution at high $K_p$. Even at $K_p = 9$ (the highest possible value), however, Eq. (9) gives 7.4 kV/$R_E$, which is only approximately 65% higher than expected at $K_p = 7$. Thus Eq. (9) will not diverge noticeably across the $K_p$ for which it will be used, even though it is a cubic function.

### 3.3. Equatorial motion obtained from the E5D electric field model and dipole magnetic field

The $\mathbf{E} \times \mathbf{B}$ drift angular and radial velocities ($v_\theta$ and $v_r$) in the magnetic equatorial plane that result from using the E5D electric field model and a Earth centered offset dipole magnetic field are (in km/s)

$$v_\theta = (10^3 B R_E)^{-1} \frac{\partial G}{\partial R}, \tag{10}$$

$$v_r = -(10^3 B L R_E)^{-1} \frac{\partial G}{\partial \theta}, \tag{11}$$

$$\frac{\partial G}{\partial R} = \frac{\partial G_1}{\partial R} G_2 J + G_1 \frac{\partial G_2}{\partial R} J + G_1 G_2 \frac{\partial J}{\partial R} + \frac{\partial G_3}{\partial R}, \tag{12}$$

$$\frac{\partial G_1}{\partial R} = V_1 \sin(\theta) + V_2 \cos(\theta), \tag{13}$$

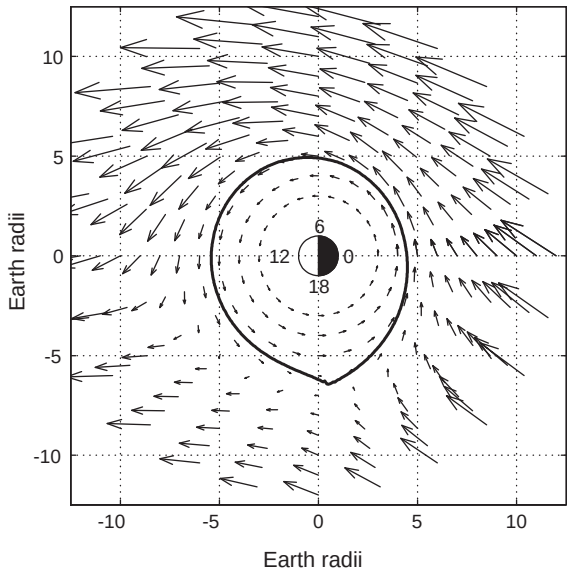


Fig. 1. $K_p = 3$ velocity vectors due to $\mathbf{E} \times \mathbf{B}$ drift in the magnetic equatorial plane obtained from the E5D electric field potential and a dipole magnetic field. The last closed equipotential for $K_p = 3$ is shown by the solid line, as well as the locations of 0, 6, 12, and 18 MLT.

$$\frac{\partial G_2}{\partial R} = 0, \tag{14}$$

$$\frac{\partial G_3}{\partial R} = V_5/R^2, \tag{15}$$

$$\frac{\partial J}{\partial R} = J^2 \left(\frac{\gamma}{R}\right) \left(\frac{V_6 R_{ar}}{R}\right)^\gamma, \tag{16}$$

$$\frac{\partial G}{\partial \theta} = \frac{\partial G_1}{\partial \theta} G_2 J + G_1 \frac{\partial G_2}{\partial \theta} J + G_1 G_2 \frac{\partial J}{\partial \theta} + \frac{\partial G_3}{\partial \theta}, \tag{17}$$

$$\frac{\partial G_1}{\partial \theta} = R[V_1 \cos(\theta) - V_2 \sin(\theta)] \tag{18}$$

$$\frac{\partial G_2}{\partial \theta} = 0, \tag{19}$$

$$\frac{\partial G_3}{\partial \theta} = 0, \tag{20}$$

$$\frac{\partial J}{\partial \theta} = \gamma \sin(\theta) J^2 \left(\frac{V_6 R_{ar}}{R}\right)^\gamma \left(\frac{S_2 + S_4 K_L}{R_{ar}}\right). \tag{21}$$

Fig. 1 shows the velocity vectors obtained with the above equations and the location of the last closed equipotential when $K_p = 3$.

To determine the streamline of a plasma element in the magnetic equatorial plane Eqs. (10) and (11) need to be solved numerically, using small time steps. GPID uses time steps of 50 s. Within each time step, the changes in $L$ and MLT are given by

$$\Delta L = \Delta t(v_r/R_E) \quad \Delta \mathrm{MLT} = \Delta t(v_\theta/L R_E). \tag{22}$$

Plasma on closed equipotential surfaces orbit Earth in an eastward direction. Plasma on open equipotentials will flow from the magnetotail in a sunward direction past the Earth, towards the magnetopause. Because GPID uses 3-hourly $K_p$ data, which often varies between each 3-hourly period, a well defined plasmapause will generally not occur at the last closed $\mathbf{E} \times \mathbf{B}$ equipotential at a given instant in time. The exception is during the onset of a large geomagnetic storm, when an extended period of high $K_p$ will result in the plasmapause being carved out on the night side from the (potentially) saturated plasmasphere (e.g., Lemaire and Gringauz, 1998). As the storm, and hence $K_p$, subsides the plasmapause will remain a prominent feature but it will occur inside the new location of the last closed equipotential (Fig. 1). A model such as GPID, however, can follow this very dynamic evolution of the plasmasphere and the density structures of which it is composed.

### 3.4. Magnetic flux tubes

GPID assumes that $v_\theta$ and $v_r$ in the magnetic equatorial plane control the motion of the plasma contained within the entire corresponding magnetic flux tube. GPID uses two main steps in each $\Delta t$ to follow the evolution of the global plasmasphere. First, it determines the change in $H^+_{tot}$ of each magnetic flux tube, using the parameters such as $T_e$ and $n_e$ at the initial location of each flux tube using the approach described in Webb and Essex (2001). Second, it then moves each of the plasma tubes to a new location determined by Eq. (22).

To maintain a consistent spread of plasma tubes, GPID uses a uniformly spaced $L$-MLT grid given by

$$L = (1 + 400/R_E), 1.1, 1.15, 1.2, 1.3, 1.4, \ldots, 6.7, 6.8, 7.0,$$

$$7.2, \ldots, 9.0,$$

$$\mathrm{MLT} = 0.0, 0.5, 1.0, \ldots, 23.0, 23.5,$$

which gives a total of 3408 plasma tubes. The $L$ separations are increased beyond $L = 6.8$, as this corresponds to just beyond the location of geostationary orbit. This represents the greatest distance from which plasmaspheric TEC data can generally be obtained and, hence, high resolution spatial variations are not needed. Furthermore, the accuracy of GPID becomes increasingly questionable at higher $L$. The main reasons are (1) the increasing inaccuracy of the dipole magnetic field model at these locations, especially during periods of increased geomagnetic activity, and (2) the dipole field does not model the effects of the magnetopause, which occurs around $\sim 10\ R_E$ (e.g., Shue et al., 2000). The approach used by GPID is easily scalable to a finer grid and/or a greater number of field line divisions, if the computer resources are available.

The offset-centered dipole magnetic field (Kivelson and Russell, 1995) is used by GPID as a computationally simple approximation to the Earth's true magnetospheric field. One future improvement to GPID will be to replace the dipole magnetic field with the more physically realistic 1996 or 2001 Tsyganenko models (T96 or T01) (Tsyganenko, 1996, 2002a,b). While the use of T96 or T01 should not greatly affect the GPID predictions within the inner plasmasphere (say, $L < 3$–4), except during very severe geomagnetic storms (Tsyganenko et al., 2003), their use will increase the accuracy of GPID at higher $L$. This increased accuracy could have important consequences in how well GPID predicts the distribution of plasma in the outer plasmasphere that is being ripped away during the onset of a geomagnetic storm. Also, it will introduce potentially important diurnal variations that are absent from the dipole approach.

### 3.5. Compression and rarefaction

Murphy et al. (1980) noted that a magnetic flux tube is defined 'by specifying the amount of magnetic flux passing through it', with the same flux used for all tubes. The magnetic flux $\Phi$ is

$$\Phi = BA, \tag{23}$$

where $A$ is the cross sectional area in $m^2$, and $B$ is the magnetic field strength in $T$. All tubes in GPID have a flux equal to that at 350 km altitude passing through an area of 1 $m^2$ along an $L = 3$ field line, which gives a standard magnetic flux of $\Phi_s = 4.44 \times 10^{-5}$ $Tm^2$. In a dipole magnetic field the volume of a flux tube ($V_L$) with standard magnetic flux $\Phi_s$ is

$$V_L = \frac{32 R_E L^4 \Phi_s}{35 B_o} \left(\sqrt{1 - V_p}\right) \times \left(1 + \frac{1}{2} V_p + \frac{3}{8} V_p^2 + \frac{5}{16} V_p^3\right), \tag{24}$$

where $B_o = 30.4 \times 10^{-6}$ T (Kivelson and Russell, 1995, p. 305), $V_p = r_o/LR_E$, and $r_o = R_E + 350$ km. When $r_o = R_E$ and $\Phi_s = 1$ $Tm^2$, Eq. (24) agrees with the expression presented by Rasmussen et al. (1993).

While the concept of conserved magnetic flux allows for the expansion and compression of a single tube of plasma as it rotates around the Earth, it does not take into account the possible interactions between adjacent plasma tubes. For example, in regions where plasma tubes are slowing down adjacent plasma tubes along an equipotential surface will 'pile up', while in regions where acceleration is occurring the plasma tubes will separate. Since the plasma tubes are representative of a continuous plasma, these situations correspond to net increases or decreases in the plasma tube content, respectively.

To include these effects in GPID the following approach is used. For each plasma tube, at a given $L$ and MLT, it is assumed that the initial cross-sectional area is square in the magnetic equatorial plane centered on the field line, with the area of the square given by Eq. (23). The coordinates of the square's vertices in $L$ and MLT are determined and their

new coordinates, after $\Delta t$, calculated. From the vertices new coordinates the cross-sectional area of the plasma tube is determined, and is compared to the expected cross-sectional area given by Eq. (23). The new plasma tube content is corrected by dividing the original content by the ratio of the two areas. If this ratio is greater than one, the plasma tubes have spread out and the plasma tube content will decrease. If the ratio is less than one, the plasma tubes have piled up, and the plasma tube content will increase.

### 3.6. Background content

The 'background' density is the minimum allowable equatorial $n_e$ and in GPID it is assumed to be equal to the equatorial plasmatrough $n_e$ (e.g., Carpenter and Anderson, 1992; Gallagher et al., 1998). Taking the equatorial $n_e$ to be equal to $n_{eq}(H^+)$, an approximate value for the minimum $H^+_{tot}$ can be found by multiplying the $n_{eq}(H^+)$ by $V_L$, i.e., this assumes that $n_e$ is constant along the flux tube. It should be noted, however, that the field-aligned $n_e$ is always calculated using the diffusive equilibrium approached discussed in Webb and Essex (2001), even when the background equatorial $n_e$ is used. GPID uses the plasmatrough equatorial density expression from Carpenter and Anderson (1992), which at MLT = 0 reduces to (in $cm^{-3}$)

$$n_e(L) = 5800L^{-4.5} + [1 - \exp(-[L-2]/10)]. \quad (25)$$

### 3.7. Interpolation procedure used by GPID

GPID maintains the required $L$-MLT grid by starting with the grid specified in 3.4 and then determining the location of each grid point after $\Delta t$. Interpolation is then used to map the $H^+_{tot}$ values onto the initial $L$-MLT grid. In this way a uniform distribution of plasma tubes is maintained after each time interval. Fig. 2 shows the location of each plasma tube in the $L$-MLT grid after $\Delta t$ of 1 h when $K_p = 3$. Points with $L < 2$ have simply corotated, and have been removed for clarity. As this demonstrates, even after only 1 h some regions of the original $L$-MLT grid on the nightside have become depopulated of plasma tubes. It is, therefore, not possible to use interpolation in these regions. GPID solves this problem by adding two 'rings' of plasma tubes at $L = 1$ and $L = 9$ at the same MLT as the $L$-MLT grid, as well as plasma tubes radially outside the new locations of the original $L = 9$ tubes. The plasma tubes on the $L = 1$ ring are assumed to have a $H^+_{tot}$ equal to the inner tube of each corresponding MLT, while the other added plasma tubes on the outer ring and radial outside the $L = 9$ tubes are all assumed to have $H^+_{tot}$ equal to the background content given by Eq. (25). In the nightside 18 MLT to 6 MLT region the plasma tubes with $H^+_{tot}$ equal to the background represent empty flux tubes that have moved sunward from the magnetotail. Plasma tubes that move outside $L = 9$ are considered lost.

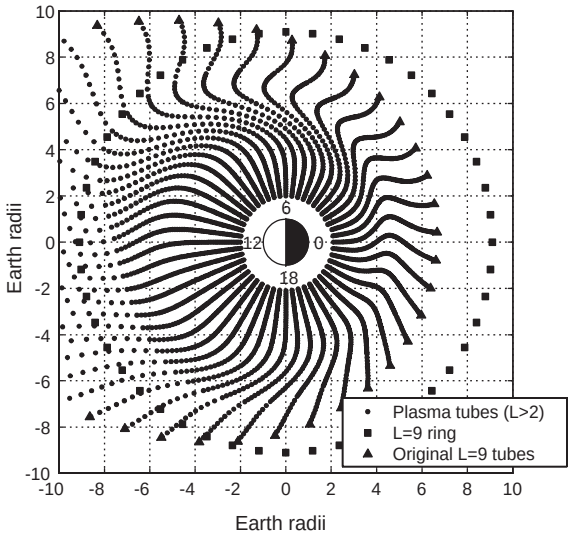


Fig. 2. Locations of plasma tubes after 1 h of motion from the initial uniform $L$-MLT grid, when $K_p = 3$. Also shown are the outer rings of points required for interpolation, as well as the locations of 0, 6, 12 and 18 MLT.

One of the main problems with using this approach is the use of interpolation. Interpolation repeated multiple times has the effect of smoothing out density features such as the plasmapause. The best solution to retain sharp features such as the plasmapause is to use 'nearest-neighbour' interpolation, where the value of the nearest point in the data set been interpolated is used for the interpolated value, which does not suffer from this smoothing problem.

### 3.8. The polar regions

The primary aim of the GPID polar method is to model the main plasmasphere $n_e$ features, and to smoothly join the polar densities to the plasmasphere model. Because of the complex nature of the polar wind flow at high latitudes (e.g., Schunk, 1983, 1988, 2000), it is computationally unrealistic for GPID to use a physics-based model for the polar regions. Rather, a simplified empirical approach is used since, as previously noted, GPID was originally designed to estimate the plasmaspheric contribution to TEC measurements. Since $n_e$ in the plasmasphere is generally one to two orders of magnitude higher than in the plasmatrough and polar regions (e.g., Carpenter and Anderson, 1992; Gallagher et al., 2000; Nsumei et al., 2003), the accuracy of the approach used by GPID to model theses regions does not have to be high (say, ±50%). The GPID polar and plasmatrough $n_e$ predictions become much more important if comparisons are made to in-situ or remote density measurements such as those from the Radio Plasma Imager Instrument (RPI) on the IMAGE satellite (Reinisch et al., 2001a).

In GPID a closed magnetic field line is broken up into logarithmically spaced sections, between the base height of

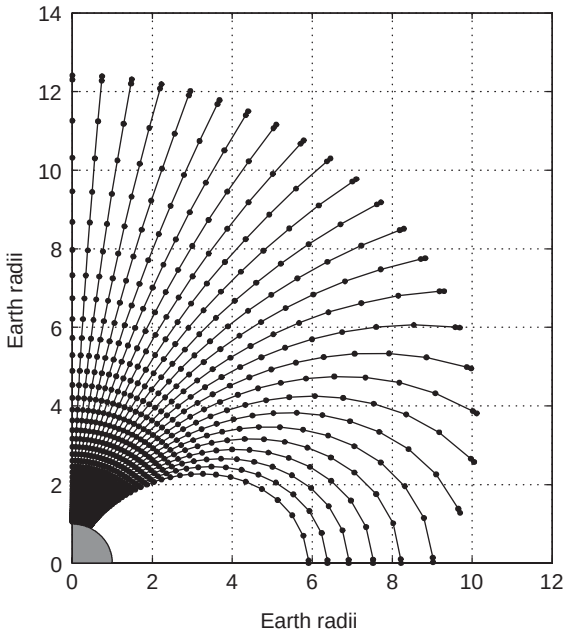


Fig. 3. Variation in the interval spacing, denoted by the circles, used along polar magnetic field lines from $\Lambda = 65°$ to 90°. The field lines are broken into sections equal to the total length of an $L = 9$ field line.

350 km and the field line apex. This approach is used up to $L = 9$. For field lines corresponding to $L > 9$, a modified logarithmically spaced sectioning of the field line is used. Rather than breaking up the total length of the field line, it is broken up between the base height and the distance along the field line equal to the length of a $L = 9$ field line. Fig. 3 shows the sectional spacing along polar field lines in 1° steps from invariant magnetic latitude $\Lambda = 65°$.

In the polar regions GPID determines the $n(O^+)$ profiles up the field lines using diffusive equilibrium, as is done at low and mid-latitudes. This gives general agreement with satellite observations (e.g., Hoffman and Dodson, 1980; Chandler et al., 1991; Kletzing et al., 1998), and results in continuous $n(O^+)$ profiles across all latitudes. Good agreement with empirical Global Core Plasma Model (GCPM) model (Gallagher et al., 2000) can be obtained by using the equatorial profile given by Eq. (25), with $L$ replaced by $R$, as shown in Fig. 4. This results in the polar and the empty flux tubes $n_e$ profiles in the plasmasphere being the same. In GPID the polar $n(H^+)$ profiles are obtained by assuming that they are equal to the empirical polar $n_e$ profile.

To produce a smooth global picture, GPID calculates polar $n(H^+)$ profiles ($n_{pol}(H^+)$) for $L > 7$, the plasmaspheric profiles for $L < 13$, and then combines the profiles between $7 < L < 13$ using a weighting function (wt) based on a general function presented in Gallagher et al. (2000). The combined profile $n_{com}(H^+)$ is given by

$$n_{com}(H^+) = n(H^+)\mathrm{wt} + n_{pol}(H^+)(1 - \mathrm{wt}) \quad (26)$$

$$\mathrm{wt} = 0.5\left[1 + \tanh\left(3.4534\,\frac{(L-10)}{3}\right)\right]. \quad (27)$$

To give better agreement with recent RPI $n_e$ observations (Nsumei et al., 2003), the currently used polar density model will need to be improved. This improvement could take the form of an empirical model based on these RPI observations, or through the use of a theoretical polar wind distribution (e.g., Schunk, 2000).

### 3.9. Running the model

The MSIS and TTM models require $F_{10.7}$ and $K_p$ as inputs, while the E5D requires $K_p$. GPID is designed to reproduce the plasmasphere on the given date required by the user. It thus includes databases of both the $F_{10.7}$ and $K_p$ values obtained from NOAA. GPID, however, can be easily modified so that a user can input a series of $F_{10.7}$ and $K_p$ values to investigate their effect on the temporal evolution of the plasmasphere. Because the $F_{10.7}$ values are daily, GPID assumes that they occur at 12 UT and then uses linear interpolation to determine the $F_{10.7}$ at the required time. This interpolation is performed so that sudden changes in $F_{10.7}$ at 0 UT do not occur, which can result in unrealistic sudden changes in the MSIS and TTM outputs. A similar interpolation is not undertaken for $K_p$ because 3-hourly $K_p$ values are used. If either the T96 or T01 magnetic field model is included in GPID, then the data sets will have to be expanded to include the solar wind and interplanetary magnetic field values required by these models.

A GPID simulation can be of two forms: a continuation of a previous run or a new run. In the case of a continuation run, GPID will use the stored results from the end of the previous run to determine the $H^+_{tot}$ values of each flux tube. For a new run GPID sets all $H^+_{tot}$ values equal to the plasmatrough density Eq. (25) multiplied by $V_L$. GPID then starts the simulation from the required date using the stored $F_{10.7}$ and $K_p$ values from its database. To evolve from the initial starting condition of a completely depleted plasmasphere, which is physically unrealistic, GPID should simulate 10–15 days before its predictions are used. If the run is a continuation of a previously completed run, however, then the results can be used from the first simulated day of the continuation run.

## 4. Comparisons with observations

### 4.1. Overview

To investigate how accurately GPID reproduces plasmaspheric and polar $n_e$ and hence plasmaspheric TEC, three separate data sets are considered. Each contain direct observations of the plasmasphere with generally little ionospheric component. This restriction is important, since a small error in the calculated ionospheric TEC can easily ‘wash out’ the

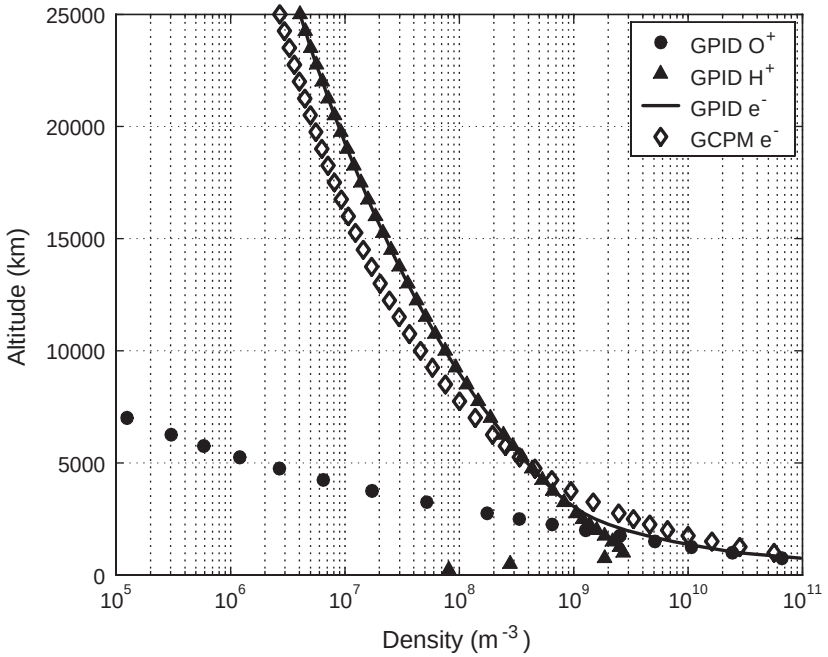


Fig. 4. Example of polar density profiles produced by GPID and the polar component of GCPM, for $\mathrm{Lon_m} = 70°$, $\Lambda = 80°$ at local midday 21 September 1999.

plasmaspheric contribution, since the ionospheric content is larger.

GPID uses the IRI model for the ionosphere, up to 50 km above the local F2 $n_e$ peak. The daily variation in the ionospheric $n_e$ is up to 35% of the mean (Forbes et al., 2000), and is primarily due to variations in the underlying neutral atmosphere. These daily effects can be categorised as meteorological changes, compared to variation in solar radiation, as determined from $F_{10.7}$, that controls the mean ionosphere over time periods of the order of weeks and months. The use of the term "meteorological" is the same as used by Forbes et al. (2000), i.e., to denoted processes that originate in the lower atmosphere but then propagate upwards to affect the ionosphere via "upward-propagating tides, planetary waves, and gravity waves". The IRI reproduces the effects of solar changes, but not the meteorological changes. Unless other daily ionospheric observations can be used to correct the IRI predictions, comparisons of daily ionospheric TEC observations with the GPID predictions are unlikely to show good agreement.

### 4.2. Ørsted

#### 4.2.1. Ørsted TEC observations

Ørsted (Oersted) is a 65 kg Danish LEO satellite in a near polar orbit with an apogee of 865 km and perigee of 649 km (e.g., Escudero et al., 2001). The Danish Meteorological Institute (DMI) provided the Ørsted data presented here.

For each continuous observation of a particular GPS satellite the resulting TEC profile is called an arc. Because of unknown phase ambiguity in each arc, the Ørsted GPS receiver can only measure relative changes in TEC. Knowledge of a constant TEC offset ($\Delta$TEC) is required to give absolute measurements. $\Delta$TEC is a fixed value, measured in TEC units (TECU), where $1\ \mathrm{TECU} = 1 \times 10^{16}\ \mathrm{e^{-}m^{-2}}$. One method to estimate $\Delta$TEC is to fit the Ørsted TEC (OTEC) observations to the GPID TEC (GTEC) prediction, using a least squares fit with a weighting equal to the inverse of the GTEC values. This weighting emphasises the TEC values that most likely correspond to direct plasmaspheric TEC observations. The $\chi^2$ function that is minimised is given by

$$\chi^2 = \sum_{i=1}^{n} \left( \frac{1}{\mathrm{GTEC}_i} \right) (\mathrm{GTEC}_i - [\mathrm{OTEC}_i + \Delta\mathrm{TEC}])^2. \tag{28}$$

#### 4.2.2. Examples of single continuous GPS observations

Fig. 5 show the orbital locations of Ørsted and a single GPS satellite, which Ørsted tracked for over 2 h on 19 November 1999. The TEC observed by Ørsted is shown in Fig. 6; the upper panel gives the complete TEC plot, and the lower panel gives a magnified view of the low TEC portion that corresponds to signal paths that only traverse the plasmasphere and not the dense ionosphere region. The upper plot shows both the original Ørsted TEC and the corrected TEC after $\Delta$TEC was calculated, which in this case was $\Delta\mathrm{TEC} = 131$ TECU.

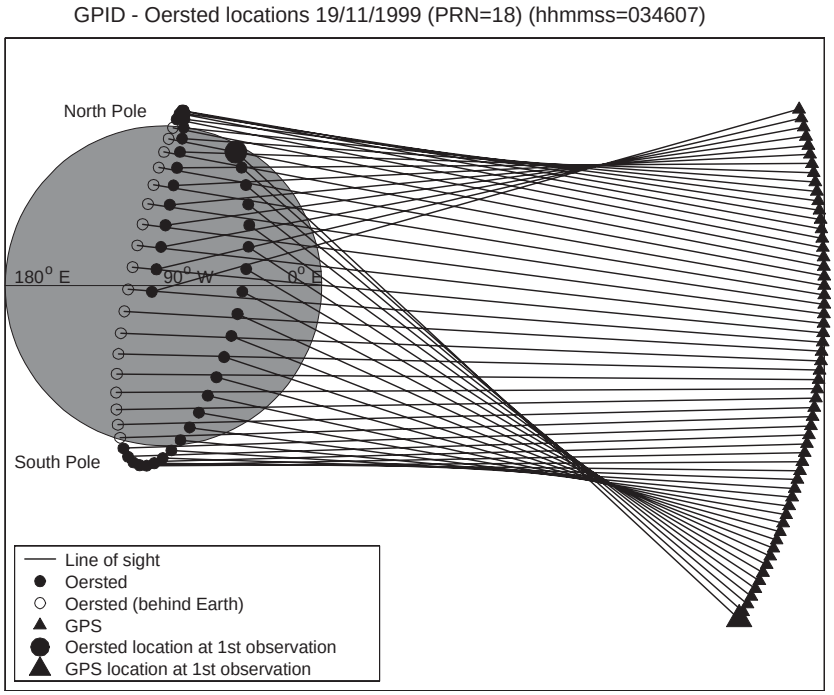


Fig. 5. Orbital locations of Ørsted and GPS satellite designated by Pseudorandom Code Number (PRN) = 18 during a continuous 2 h tracking that started at UT = 3 hr 46 min on 19 November 1999.

The very high TEC peaks correspond to ionospheric occultations, where the ray path between Ørsted and the GPS satellite passes through the ionosphere. The GPID occultation TEC will depend primarily on the IRI $n_e$ and are therefore subject to error as discussed earlier. Nevertheless, as can be seen in Fig. 6, GPID reproduces the major TEC features observed by Ørsted very well, particularly the plasmaspheric TEC values.

Because of the unknown phase ambiguity, the DMI chose to provide the Ørsted data offset so that each arc's TEC values summed to zero. This offset resulted in the 'raw' TEC data sometimes being negative, as can be seen in the upper panel of Fig. 6. A $\Delta$TEC is required for each arc to convert from relative to absolute TEC, the latter of which can only be positive. As is shown in Fig. 6, the use of Eq. (28) to determine the single $\Delta$TEC value for the entire arc can still, at times, produces absolute Ørsted TEC values that are negative and, hence, physically unreal. In the case of Fig. 6, this indicates that the GPID arc TEC predictions between $\sim$3.8–4.4 UT are probably too low and/or too high between $\sim$5.1–5.6 UT. For the purposes of comparing GPID to the Ørsted data sets, however, Eq. (28) was used because visual inspection showed it generally gave the best estimate of $\Delta$TEC for each arc.

Furthermore, in the next section only the parts of the TEC arcs with minimum ray path altitudes greater than 700 km were considered. This reduces potential errors introduced in the calculation of $\Delta$TEC by Eq. (28), since ionospheric TEC occultation values are ignored. The only way to completely avoid the problem of calculating a $\Delta$TEC value, however, is to compare the TEC gradients rather than the absolute TEC values since $\Delta$TEC is then not required. Both approaches are considered in the next section.

It should be noted that given the global nature of GPID, it cannot be expected to accurately predict the small scale TEC features obtained from a single TEC arc, such as that shown in Fig. 6. To more accurately compare GPID to the Ørsted observations, the entire data set needs to be considered. In this way small-scale variations, such as those shown in Fig. 6, will be average out and the global scale accuracy of the GPID can be more thoroughly investigated. This approach is described in the next section.

#### 4.2.3. *Comparison with full Ørsted data set*

The DMI provided 10 days of Ørsted TEC data from August through December 1999. Each Ørsted data file corresponded to an arc with TEC values observed at intervals of 10 s, normalised to a mean TEC of zero.

The observed Ørsted TEC values are compared with the GPID predictions for only those TEC values corresponding to ray paths with a minimum altitude above 700 km, which totaled 316 in number. This is useful, as these raypaths have not traversed the bulk of the ionosphere and, therefore, correspond to direct measurements of the topside ionosphere

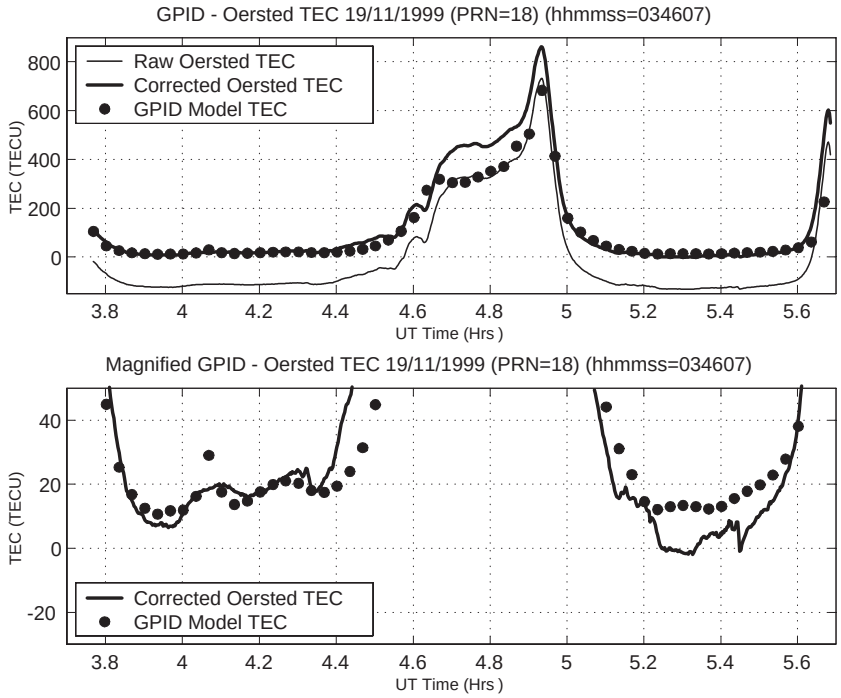


Fig. 6. Example of Ørsted TEC and the GPID prediction, corresponding to the orbits shown in Fig. 5. 'Raw' is the relative TEC, while 'Corrected' denotes the fitted TEC. The lower plot is a magnified version of the upper plot, showing the low plasmaspheric TEC features.

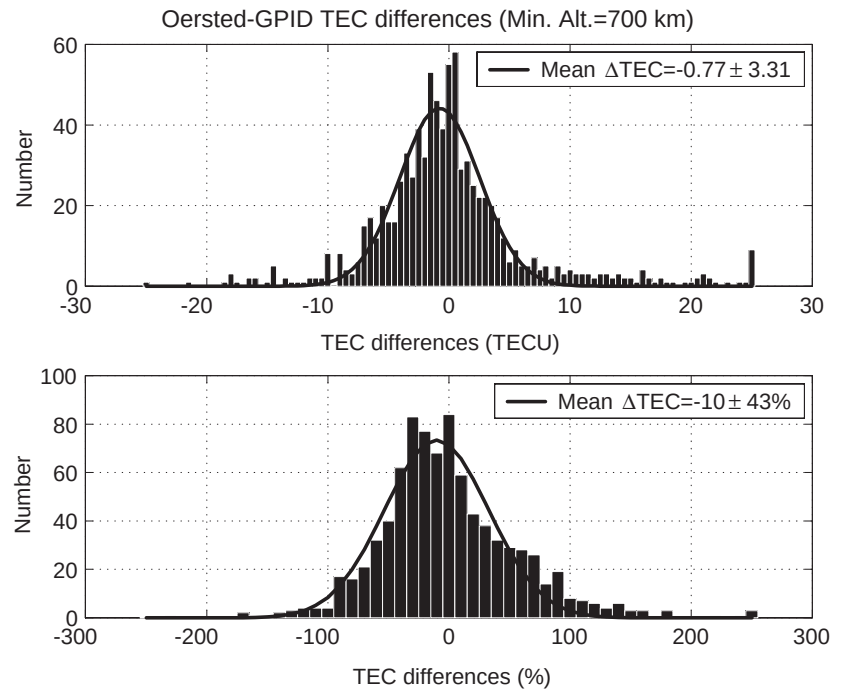


Fig. 7. Upper panel shows histogram of Ørsted TEC observations minus the GPID predictions for raypaths above 700 km, while the lower panel shows the same data as a percentage difference.

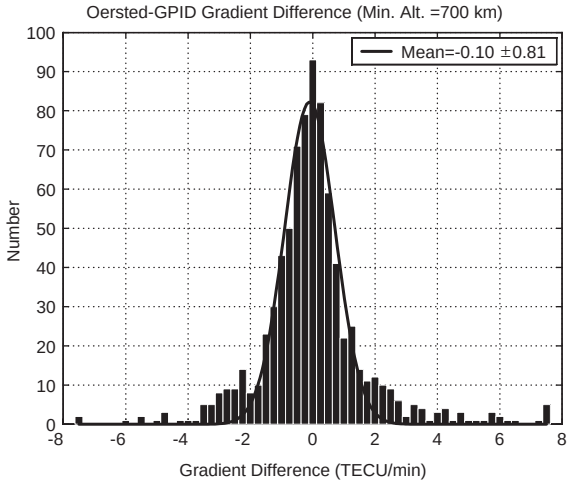


Fig. 8. Histogram of Ørsted TEC gradients minus the GPID TEC gradients for raypaths above 700 km.

and plasmasphere. Fig. 7 shows the TEC difference between the Ørsted data and the GPID predictions: the upper panel displays OTEC-GTEC and the lower panel the percentage difference $\frac{\text{OTEC}-\text{GTEC}}{\text{GTEC}}$. The mean in both cases is slightly lower than the expected value for exact agreement of zero, indicating that GPID is slightly overestimating the observed TEC.

The previous approach requires the separate calculation of ΔTEC for each arc, which introduces a possible source of error through the method used to determine this value. One approach to compare the Ørsted and GPID data that does not require ΔTEC for each arc is to compare the TEC gradients of the Ørsted arc and the corresponding GPID prediction; this is done in Fig. 8 which shows $\frac{\Delta\text{OTEC}}{\Delta\text{time}} - \frac{\Delta\text{GTEC}}{\Delta\text{time}}$, where Δtime is the time between adjacent observations. The mean is close to the expected value of zero, indicating good agreement between the model and the uncorrected observations.

### 4.3. ATS-6

The ATS-6 satellite was launched into a geostationary orbit in 1974. The ATS-6 radio beacon transmitted on multiple frequencies, allowing the TEC along the entire ray path to be calculated between the satellite and ground receivers (Davies et al., 1975). Further, by studying the Faraday rotation of the signals a separate simultaneous measurement of the ionospheric TEC could also be obtained. By subtracting the Faraday TEC from the total TEC, the plasmaspheric TEC could be determined (Kersley and Klobuchar, 1980). The ATS-6 TEC data considered here consists of hourly observations of both Faraday TEC and plasmaspheric TEC. The GPID Faraday TEC is determined using the approached described in Titheridge (1972).

Fig. 9 shows an example of the observed ATS-6 TEC at Aberystwyth, United Kingdom, the GPID prediction, and $K_p$ during May 1976. This example shows the dynamic ability of GPID to accurately model the emptying of the plasmasphere due to increased geomagnetic activity and the subsequent refilling of the depleted flux tubes.

As shown in the upper panel of Fig. 9, a very large, $K_p=8$, geomagnetic storm occurred on May 3, which was followed by an extended 16 day quiet period. The effect of the geomagnetic storm is to deplete the plasmasphere, with the TEC falling by roughly half in one day. There are two mechanisms for the depletion of the plasmaspheric TEC content in the aftermath of a storm. The first is that the plasmapause moves significantly inward, and the second is that inside the location of the new plasmapause dumping of plasma into the ionosphere can occur (e.g., Park, 1973; Carpenter and Lemaire, 1997). This depletion is followed by the refilling of the plasmasphere during the following quiet period. During the solar minimum conditions of May 1976 the fastest refilling of the plasmasphere is expected to occur, as shown in Webb and Essex (2001). Even after 16 days, however, the ATS-6 observations and GPID show that the refilling of the plasmasphere is not complete. Around May 19 the increased geomagnetic activity results in the plasmasphere being emptied by about 20%, compared to the highest observed TEC. Due to slightly higher geomagnetic activity for the remainder of the month, the plasmasphere remains in this partially depleted state.

Unlike the single flux tube refilling comparisons investigated in Webb and Essex (2001), the refilling in Fig. 9 is of the entire plasmasphere that consists of multiple flux tubes spread across a range of $L$ values. Overall, Fig. 9 shows good agreement between GPID and the ATS-6 derived plasmaspheric TEC. The basic refilling is overlaid with a diurnal variation of ±0.5 TECU, which is in agreement with Webb and Essex (2001). This agreement demonstrates that a magnetic flux tube will show diurnal variations in total content even when it reaches saturation.

Fig. 10 shows the mean values for each month at local midday and midnight for the ATS-6 and GPID plasmaspheric TEC obtained at Aberystwyth. The GPID predictions follow the TEC observed by ATS-6, showing agreement for each month to within the experimental error of one standard deviation displayed. The daytime values are about 0.5 TECU higher than those observed at night, which is in general agreement with the diurnal variations shown in Fig. 9.

The ATS-6 TEC observations and GPID show that there is little seasonal variation in the plasmaspheric TEC. Various studies have found seasonal/annual plasmaspheric density variations, though it appears that there is a longitudinal and $L$ shell dependence on the strength of the variation (e.g., Park, 1973; Park et al., 1978; Clilverd et al., 1991; Guiter et al., 1995; Richards et al., 2000; Berube et al., 2003). When a single corotating magnetic flux tube was considered, GPID produced a seasonal density variation that generally agreed with the phase of observed seasonal changes derived from

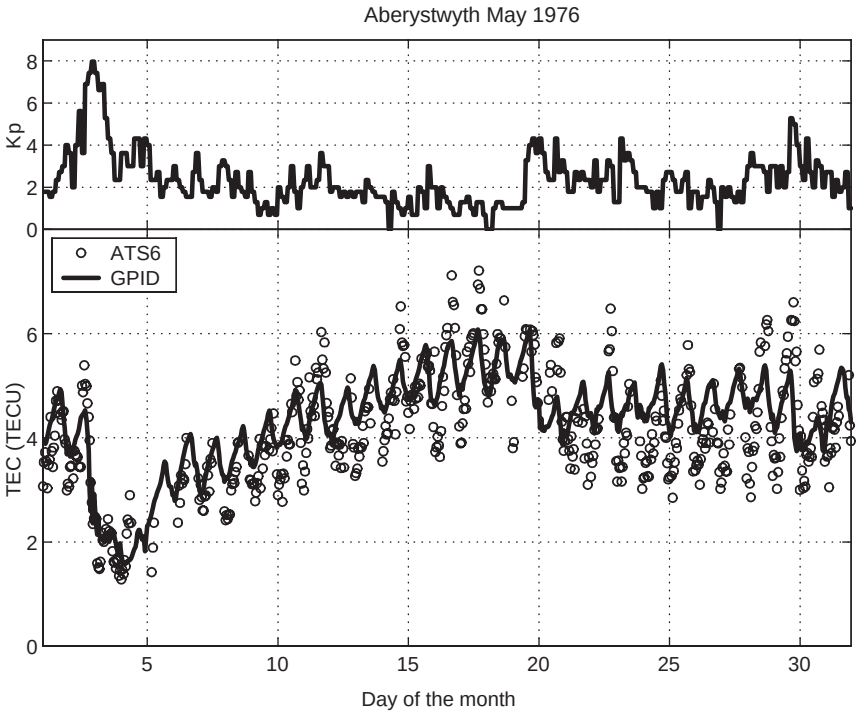


Fig. 9. Hourly ATS-6 measurements of the Faraday and plasmaspheric TEC recorded at Aberystwyth during May 1976. Also shown is $K_p$, and the GPID TEC prediction.

whistler observations (Webb and Essex, 2001). In the case shown in Fig. 10, however, the ATS-6 TEC observations and the corresponding GPID predictions show no noticeable seasonal variation. A more detailed investigation of this apparent difference between the ATS-6 observations and the other studies should be undertaken.

### 4.4. Empirical models

Comparisons have also been made between GPID and the magnetic equatorial plane $n_e$ used by two empirical models based on direct satellite measurements. The Carpenter and Anderson (1992) model is based on observations from ISEE 1 of the plasmasphere when saturated, i.e., the magnetic flux tubes are nearly full of plasma rather than in the process of refilling after being emptied by a geomagnetic storm, while the GCPM (Gallagher et al., 2000) is based on average plasmaspheric DE 1 $n_e$ equatorial observations. Fig. 11 compares these models with mean monthly GPID profiles at different $F_{10.7}$ obtained by averaging $n_e$ in the equatorial plane at 0 UT on each day of the four months displayed.

The GPID profiles show little change across the different solar fluxes, with variations at higher $L$ of only $\sim 50\%$. GPID shows very good agreement with the mean profiles of the GCPM, while it can be seen that the saturated $n_e$ profiles of Carpenter and Anderson (1992) at high $L$ are larger than the average month results. This is to be expected, since their profile is for a saturated plasmasphere and the plasmasphere is rarely saturated beyond $L > 4$.

## 5. Planned improvements to GPID

As previously discussed, some of the future improvements to GPID include: replacing the dipolar magnetic field with either the T96 or T01 model; seeking more accurate methods to simulate $n_e$ in the polar regions using either an approach based on polar wind modeling or using an empirical model based on recent RPI IMAGE observations; and replacing the E5D equatorial electric field model with the Rice MSM model.

Another point under consideration for future improvement concerns the assumed field-aligned plasma distribution. As discussed in Webb and Essex (2001), GPID uses a diffusive equilibrium approach that agrees with satellite and whistler observations, as well as the more physically complete FLIP model. Various studies, however, have shown that a diffusive equilibrium distribution is not applicable during the early refilling stages of a depleted magnetic flux tube and that some sort of collisionless profile is more appropriate (e.g., Lemaire and Gringauz, 1998). While the diffusive equilibrium approach may not accurately model the

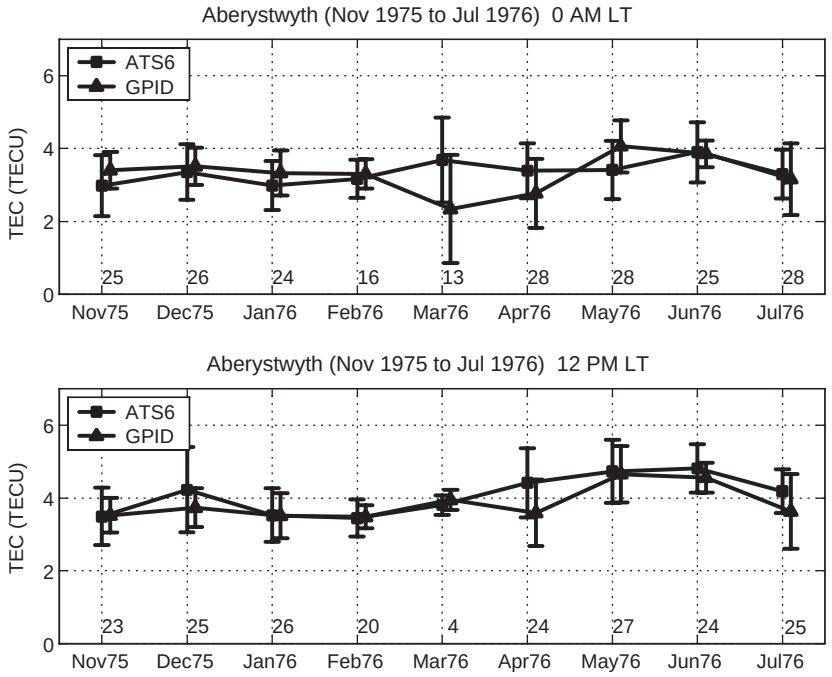


Fig. 10. Plot of the monthly mean and standard deviation in the local midnight and midday ATS-6 plasmaspheric TEC observations at Aberystwyth and the GPID predictions. The results are for the period November 1975 through July 1976. The values above each month's label are the number of ATS-6 observations available during that month for the time displayed in the plot; only the GPID predictions for the corresponding days were used to determine the GPID TEC values displayed.

field-line distribution during the early stages of refilling into the magnetic flux tube, the approach given in Webb and Essex (2001) will still accurately predict the net refilling, since this chemically driven process depends primarily on conditions in the topside ionosphere that can be accurately modeled, and not on conditions in the plasmasphere. After a few or more days of refilling (the time depends on the volume of the magnetic flux tube) the plasma distribution will convert over to a diffusive equilibrium profile and the total $H^+$ content of the magnetic flux tube will be accurately predicted by GPID.

One approach to investigate the true field-aligned distribution as the magnetic flux tube refills with ionospheric plasma would be to consider the field-aligned $n_e$ profiles that can be produced from inversion techniques applied to RPI observations from the IMAGE satellite (Reinisch et al., 2001b). These RPI-derived observations could be used to indicate at what stages of the flux tube refilling a collisionless or diffusive profile would be more appropriate, or a mixture of the two should be used.

It is also planned to apply GPID to the study of the global plasmaspheric $He^+$ images produced by the EUV Imager on IMAGE (e.g., Goldstein et al., 2003a). These images are formed by collecting solar photons resonantly scattered from the $He^+$ population. This population, however, constitutes of approximately only 10% of the plasmasphere (e.g., Lemaire and Gringauz, 1998). To compare GPID predictions with the EUV images, $He^+$ needs to be incorporated into the model. The simplest approach would be to use a previously determined empirical relation for the $He^+/H^+$ ratio that varies as a function of $R$ (Craven et al., 1997). A more desirable approach would be to include $He^+$ as a separately modeled ion species, with the field aligned distributions determined independently in a similar manner as the $H^+$. This approach would then allow the $He^+/H^+$ ratio to be investigated and compared to previous studies, as well as to the EUV Imager observations.

Many inter-calibration opportunities exist to compare GPID with observational data. For example, Webb and Essex (2001) presented comparisons with whistler observations that showed good agreement with diurnal and annual variations, and the refilling by ionospheric plasma of a magnetic flux tube refilling after a geomagnetic storm. Comparisons with empirical observations of the plasmaspheric electron density such as those obtained from POLAR measurements (e.g., Denton et al., 2002) and from $n_e$ data derived from the RPI instrument on IMAGE are planned. Also, more LEO satellite missions equipped with GPS TEC receivers are being launched (e.g., Hajj et al., 2004), providing an increasingly larger data base of plasmaspheric TEC measurements to which GPID can be compared.

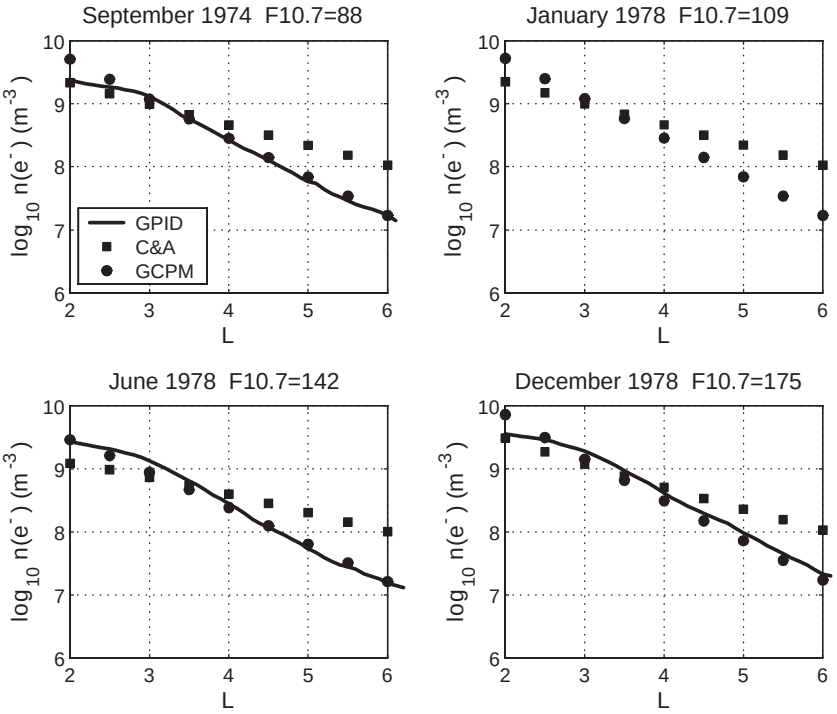


Fig. 11. Comparison between monthly averaged GPID equatorial $n_e$ profiles at 0 UT and various mean $F_{10.7}$ values, and the predictions of the empirical models of Carpenter and Anderson (1992) (C&A), and Gallagher et al. (2000) (GCPM).

## 6. Summary

The approach GPID uses to model the plasma distribution and the change in the $H^+$ flux tube content was described by Webb and Essex (2001). Here a method was described for following the time evolution of several thousand individual flux tubes distributed about the Earth, so that a global plasmasphere model can be constructed.

GPID uses a modified version of the E5D electric field model and an offset dipole magnetic field to determine the $\mathbf{E} \times \mathbf{B}$ motion in the magnetic equatorial plane of the plasma aligned in the corresponding magnetic flux tube. The physical modeling approach allows GPID to simulate diurnal, seasonal, geographic, and geomagnetic storm effects. In a relatively short time, GPID can simulate the global plasmasphere, out to an altitude of $\sim 50,000$ km, for periods of weeks or months on a desktop personal computer.

The use of the term dynamic is used to differentiate GPID from a simple static plasmaspheric model, i.e., one that does not evolve with time as geomagnetic conditions change. In addition, the model is not self-consistent due to the number of approximations used. The use of nearest-neighbour interpolation to determine the magnetic flux-tube plasma content on the $L$-MLT grid after each time step means that the total number of $H^+$ across the entire plasmasphere is not conserved. In the end, however, GPID provides an approximation of the real plasmasphere and its usefulness as a research tool is demonstrated by the ability to reproduce observational data. GPID was shown to compare favourably with different direct plasmaspheric TEC measurements derived from GPS radio signal phase changes observed by the Ørsted LEO satellite, as well as Faraday-rotation derived plasmaspheric TEC measurements from ATS-6. Similarly, comparisons with two plasmasphere empirical models gave good agreement across a large portion of the solar cycle.

The aim in developing GPID was to produce a global scale model of the plasmasphere that would allow the plasmaspheric contribution to TEC measurements between GPS satellites and ground receivers to be predicted and removed, so allowing the remaining ionospheric TEC values to be determined. As a result, GPID should only currently be used for TEC predictions and global-scale electron-density profiles. GPID does not produce accurate local density predictions, especially in the polar regions. The polar region densities are one to two orders of magnitude lower than in the plasmasphere, however, and any errors in GPID density predictions should not affect its ability to accurately predict polar TEC. Comparisons with GPS and ATS-6 TEC observations, as well as average electron density profiles, indicate that GPID is accurate out to approximately geosynchronous orbit. Planned improvements, such as including the Tsyganenko magnetic field model and the Rice MSM convection model and updating the polar density model, will make the GPID density predictions even more accurate.

## Acknowledgements

This research was supported by an ARC grant. P. Webb was supported by a La Trobe University Postgraduate Award (LUPA) and the Cooperative Research Centre for Satellite Systems (CRCSS). P. Webb is currently supported by a National Research Council (NRC) Research Associateship award at NASA/GSFC. The authors wish to thank the Danish Meteorological Institute for kindly providing the GPS-derived TEC data from the Ørsted satellite. Furthermore, we would like to thank Jack Klobuchar of Innovative Solutions International and Pat Doherty from the Institute for Scientific Research, Boston College for providing the ATS-6 TEC data. Our special thanks to Robert F. Benson (NASA/GSFC) and Joseph Grebowsky (NASA/GSFC) for helpful comments during the preparation of this manuscript. The initial stimulation for this research was provided by J. Klobucher.

## References

Bailey, G.J., Balan, N., Su, Y.Z., 1997. The Sheffield University plasmasphere ionosphere model—a review. Journal of Atmospheric and Solar-Terrestrial Physics 59, 1541–1552.

Berube, D., Moldwin, M.B., Weygand, J.M., 2003. What is the source of observed annual variations in plasmaspheric density? Journal of Geophysical Research 108 (A9), 1348. doi:10.1029/2002JA009737.

Bilitza, D., 2001. International reference ionosphere 2000. Radio Science 36, 261–275.

Brice, N.M., 1967. Bulk motion of the magnetosphere. Journal of Geophysical Research 72, 5193–5211.

Carpenter, D.L., Anderson, R.R., 1992. An ISEE/whistler model of equatorial electron density in the magnetosphere. Journal of Geophysical Research 97, 1097–1108.

Carpenter, D.L., Lemaire, J., 1997. Erosion and recovery of the plasmasphere in the plasmapause region. Space Science Reviews 80, 153–179.

Chandler, M.O., Waite, J.H., Moore, T.E., 1991. Observations of polar ion outflows. Journal of Geophysical Research 96, 1421–1428.

Ciraolo, L., Spalla, P., 1997. Comparison of ionospheric total electron content from the navy navigation satellite system and the GPS. Radio Science 32, 1071–1080.

Clilverd, M.A., Smith, A.J., Thomson, N.R., 1991. The annual variation in quiet time plasmaspheric electron density, determined from whistler mode group delays. Planetary and Space Science 39, 1059–1067.

Craven, P.D., Gallagher, D.L., Comfort, R.H., 1997. Relative concentration of $He^+$ in the inner magnetosphere as observed by the DE 1 retarding ion mass spectrometer. Journal of Geophysical Research 102, 2279–2289.

Davies, K., 1980. Recent progress in satellite radio beacon studies with particular emphasis on the ATS-6 radio beacon experiment. Space Science Reviews 25, 357–430.

Davies, K., Fritz, R.B., Grubb, R.N., Jones, J.E., 1975. Some early results from the ATS-6 radio beacon experiment. Radio Science 10, 785–799.

Denton, R.E., Goldstein, J., Menietti, J.D., Young, S.L., 2002. Magnetospheric electron density model inferred from polar plasma wave data. Journal of Geophysical Research 107 (A11), 1386. doi:10.1029/2001JA009136.

Doherty, P.H., Anderson, D.N., Klobuchar, J.A., 1997. Total electron content over the pan-american longitudes: March–April 1994. Radio Science 32, 1597–1605.

Escudero, A., Schlesier, A.C., Rius, A., Flores, A., Rubek, F., Larsen, G.B., Sysdergaard, S., Høeg, 2001. Ionospheric tomography using Ørsted GPS measurements—preliminary results. Physics and Chemistry of the Earth (A) 26, 173–176.

Forbes, J.M., Palo, S.E., Zhang, X., 2000. Variability of the ionosphere. Journal of Atmospheric and Solar-Terrestrial Physics 62, 685–693.

Gallagher, D.L., Craven, P.D., Comfort, R.H., 1998. A simple model of magnetospheric trough total density. Journal of Geophysical Research 103, 9293–9297.

Gallagher, D.L., Craven, P.D., Comfort, R.H., 2000. Global core plasma model. Journal of Geophysical Research 105, 18819–18834.

Goldstein, J., Spiro, R.W., Reiff, R.A., Wolf, R.A., Sandel, B.R., Freeman, J.W., Lambour, R.L., 2002. IMF-driven overshielding electric field and the origin of the plasmaspheric shoulder of May 24, 2000. Geophysical Research Letters 29 (16), doi:10.1029/2001GL014534.

Goldstein, J., Spasojević, M., Reiff, R.A., Sandel, B.R., Forrester, W.T., Gallagher, D.L., Reinisch, B.W., 2003a. Identifying the plasmapause in IMAGE EUV data using IMAGE RPI in situ steep density gradients. Journal of Geophysical Research 108 (A4), 1147. doi:10.1029/2002JA009475.

Goldstein, J., Spiro, R.W., Sandel, B.R., Wolf, R.A., Su, S.-Y., Reiff, R.A., 2003b. Overshielding event of 28–29 July 2000. Geophysical Research Letters 30 (8), 1421. doi:10.1029/2002GL016644.

Guiter, S.M., Rasmussen, C.E., Gombosi, T.I., Sojka, J.J., Schunk, R.W., 1995. An automated method for the detection of field line resonance frequencies using ground magnetometer techniques. Journal of Geophysical Research 100, 8013–8020.

Hajj, G.A., Ao, C.O., Iijima, B.A., Kuang, D., Kursinski, E.R., Mannucci, T., Meehan, K., Romans, L.J., de la Torre Juarez, M., Yunck, T.P., 2004. CHAMP and SAC-C atmospheric occultations results and intercomparisons. Journal of Geophysical Research 109, D06109. doi:10.1029/2003JD003909.

Hedin, A.E., 1991. Extension of the MSIS thermospheric model into the middle and lower atmosphere. Journal of Geophysical Research 96, 1159–1172.

Hoffman, J.H., Dodson, W.H., 1980. Light ion concentrations and fluxes in the polar regions during magnetically quiet times. Journal of Geophysical Research 85, 626–632.

Hofmann-Wellenhof, B., Lichtenegger, H., Collins, J., 1997. GPS Theory and Practice, 4th Edition. Springer, Berlin.

Horvath, I., Essex, E.A., 2000. Using observations from the GPS and TOPEX satellites to investigate night-time TEC enhancements at mid-latitudes in the southern hemisphere during a low sunspot number period. Journal of Atmospheric and Solar-Terrestrial Physics 62, 371–391.

Kersley, L., Klobuchar, J.A., 1980. Stormed associated protonspheric depletion and recovery. Planetary and Space Science 28, 453–458.

Kivelson, M.G., Russell, C.T. (Eds.), 1995. Introduction to Space Physics. Cambridge University Press, Cambridge.

Kletzing, C.A., Mozer, F.S., Torbert, R.B., 1998. Electron temperature and density at high latitude. Journal of Geophysical Research 103, 14837–14845.

Lemaire, J.F., Gringauz, K.I., 1998. The Earth's Plasmasphere. Cambridge University Press, Cambridge.

Liemohn, M.W., Kozyra, J.U., Thomsen, M.F., Roeder, J.L., Lu, G., Borovsky, J.E., Cayton, T.E., 2001. Dominant role of the asymmetric ring current in producing the stormtime *Dst**. Journal of Geophysical Research 106, 10883–10904.

Lunt, N., Kersley, L., Bailey, G.J., 1999a. The influence of the protonsphere on GPS observations: models simulations. Radio Science 34, 725–732.

Lunt, N., Kersley, L., Bishop, G.J., Mazzella, A.J., 1999b. The contribution of the protonsphere to GPS total electron content: experimental measurements. Radio Science 34, 1273–1280.

Mannucci, A.J., Iijima, B.A., Sparks, L.C., Pi, X., Wilson, B.D., Lindqwister, U.J., 1999. Assessment of global TEC mapping using a three-dimensional electron density model. Journal of Atmospheric and Solar-Terrestrial Physics 61, 1227–1236.

McIlwain, C.E., 1961. Co-ordinates for mapping the distribution of magnetically trapped particles. Journal of Geophysical Research 66, 3681–3691.

McIlwain, C.E., 1986. A $K_p$ dependent equatorial electric field model. Advances in Space Research 6, 187–197.

Murphy, J.A., Bailey, G.J., Moffett, R.J., 1980. A theoretical study of the effects of quiet-time electromagnetic drifts on the behaviour of thermal plasma at mid-latitudes. Journal of Geophysical Research 85, 1979–1986.

Nishida, A., 1966. Formation of plasmapause, or magnetospheric plasma knee, by the combined action of magnetospheric convection and plasma escape from the tail. Journal of Geophysical Research 71, 5669–5679.

Nsumei, P.A., Huang, X., Reinisch, B.W., Song, P., Vasyliunas, V.M., Green, J.L., Fung, S.F., Benson, R.F., Gallagher, D.L., 2003. Electron density distribution over the northern polar region deduced from IMAGE/radio plasma imager sounding. Journal of Geophysical Research 108 (A2), 1078. doi:10.1029/2002JA009616.

Park, C.G., 1973. Whistler observations of the depletion of the plasmasphere during a magnetospheric substorm. Journal of Geophysical Research 78, 672–683.

Park, C.G., Carpenter, D.L., Wiggin, D.B., 1978. Electron density in the plasmasphere: whistler data on solar cycle, annual, and diurnal variations. Journal of Geophysical Research 83, 3137–3144.

Picone, J.M., Hedin, A.E., Drob, D.P., 2002. NRLMSISE-00 empirical model of the atmosphere: statistical comparisons and scientific issues. Journal of Geophysical Research 107 (A12), 1468. doi:10.1029/2001JA009430.

Poulter, E.M., Hargreaves, J.K., Bailey, G.J., Moffett, R.J., 1981. Electron content modelling: the significance of protonspheric content. Planetary and Space Science 29, 869–883.

Rasmussen, C.E., Guiter, S.M., Thomas, S.G., 1993. A two-dimensional model of the plasmasphere: refilling time constants. Planetary and Space Science 41, 35–43.

Reinisch, B.W., Huang, X., Haines, D.M., Galkin, I.A., Green, J.L., Benson, R.F., Fung, S.F., Taylor, W.W.L., Reiff, P.H., Gallagher, D.L., Bougeret, J.-L., Manning, R., Carpenter, D.L., Boardsen, S.A., 2001a. First results from the radio plasma imager on IMAGE. Journal of Geophysical Research 28, 1167–1170.

Reinisch, B.W., Huang, X., Song, P., Sales, G.S., Fung, S.F., Green, J.L., Gallagher, D.L., Vasyliunas, V.M., 2001b. Plasma density distribution along the magnetospheric field: RPI observations from IMAGE. Journal of Geophysical Research 28, 4521–4524.

Richards, P.G., Buonsanto, M.J., Reinisch, B.W., Holt, J., Fennelly, J.A., Scali, J.A., Comfort, R.H., Germany, G.A., Spann, J., Brittnacher, M., Fok, M.C., 2000. On the relative importance of convection and temperature on the behaviour of the ionosphere in North America during January 6–12, 1997. Journal of Geophysical Research 105, 12763–12776.

Schunk, R.W., 1983. The terrestrial ionosphere. In: Carvillano, R.L., Forbes, J.M. (Eds.), Solar Terrestrial Physics. Reidel, Dordrecht, pp. 609–676.

Schunk, R.W., 1988. The polar wind. AGU Geophysical Monograph 44, 219–228.

Schunk, R.W., 2000. Theoretical developments on the causes of ionospheric outflow. Journal of Atmospheric and Solar-Terrestrial Physics 62, 399–420.

Shue, J.H., Song, P., Russell, C.T., Chao, J.K., Yang, Y.H., 2000. Toward predicting the position of the magnetopause within geosynchronous orbit. Journal of Geophysical Research 105, 2641–2656.

Singh, N., Horwitz, J.L., 1992. Plasmasphere refilling: recent observations and modeling. Journal of Geophysical Research 97, 1049–1079.

Stern, D., 1975. The motion of a proton in the equatorial magnetosphere. Journal of Geophysical Research 80, 595–599.

Titheridge, J.E., 1972. Determination of ionospheric electron content from the Faraday rotation of geostationary satellite signals. Planetary and Space Science 20, 353–369.

Titheridge, J.E., 1998. Temperatures in the upper ionosphere and plasmasphere. Journal of Geophysical Research 103, 2261–2277.

Torr, M.R., Torr, D.G., Richards, P.G., Yung, S.P., 1990. Mid- and low-latitude model of thermospheric emissions 1 $O^+(2P)$ 7320 A and N2 (2P) 3371 A. Journal of Geophysical Research 95, 21147–21168.

Tsyganenko, N.A., 1996. Modeling the global magnetic field of the large-scale Birkeland current systems. Journal of Geophysical Research 101, 27187–27198.

Tsyganenko, N.A., 2002a. A model of the near magnetosphere with a dawn–dusk asymmetry: 1. mathematical structure. Journal of Geophysical Research 107 (A8), doi:10.1029/2001JA000219.

Tsyganenko, N.A., 2002b. A model of the near magnetosphere with a dawn–dusk asymmetry: 2. parameterization and fitting to observations. Journal of Geophysical Research 107 (A8), doi:10.1029/2001JA000220.

Tsyganenko, N.A., Singer, H.J., Kasper, J.C., 2003. Storm-time distortion of the inner magnetosphere: how serve can it get? Journal of Geophysical Research 108 (A5), 1209. doi:10.1029/2002JA009808.

Tu, J.-N., Horwitz, J.L., Song, P., Huang, X.-Q., Reinisch, B.W., Richards, P.G., 2003. Simulating plasmaspheric field-aligned density profiles measured with IMAGE/RPI: effects of plasmasphere refilling and ion heating. Journal of Geophysical Research 108 (A1), 1017. doi:10.1029/2002JA009468.

Volland, H., 1973. A semiempirical model of large-scale magnetospheric electric fields. Journal of Geophysical Research 78, 171–180.

Webb, P.A., Essex, E.A., 2001. A dynamic diffusive equilibrium model of the ion densities along plasmaspheric magnetic flux tubes. Journal of Atmospheric and Solar-Terrestrial Physics 63, 1249–1260.

Webb, P.A., Essex, E.A., 2003. Modifications to the Titheridge upper ionosphere and plasmasphere temperature model. Journal of Geophysical Research 108 (A10), 1359. doi:10.1029/2002JA009754.

Webb, P.A., Liemohn, M.W., 2004. Empirical relationship between $K_p$ and the magnetospheric dawn-to-dusk electric field. Journal of Atmospheric and Solar-Terrestrial Physics, submitted.

Wilson, G.R., Horwitz, J.L., Lin, J., 1992. A semikinetic model for early stage plasmasphere refilling 1. effects of coulomb collisions. Journal of Geophysical Research 97, 1109–1119.